Efficient Numerical Optimization of Induction Machines by Scaled FE Simulations

Martin Nell, Jonas Lenz and Kay Hameyer, *Senior Member, IEEE*

***Abstract*—In this paper a scaling methodology for the solution of 2D FE models of electric machines is proposed. This allows a geometrical and rotor resistance scaling of a squirrel cage induction machine enabling an efficient numerical optimization. The 2D FEM solutions of a reference machine are calculated by a model based hybrid numeric induction machine simulation approach. In contrast to already known scaling procedures for synchronous machines the FEM solutions of the induction machine are scaled in the stator-current-rotor-frequency-map and then transformed into the torque-speed-map. This gives the possibility to use a new time-scaling factor, that is necessary to keep a constant field distribution. The scaling procedure is validated by the finite-element-method and used in a numerical optimization process for the sizing of an electric vehicle traction drive considering the gear ratio. The results show that the scaling procedure is very accurate, computational very efficient and suitable for the use in machine design optimization.**

***Index Terms*—Induction machine, induction motor, scaling laws, finite-element method analysis, loss-calculation, multi-objective optimization, Evolutionary Strategy, efficiency map**

I. Introduction

Energy optimization performed for example by an improvement in efficiency of electrical equipment is the global trend today [1]. In developed countries the industrial induction machines (IM) are the major consumers of electric energy and globally account for about $40\,\%$ if overall power consumption [2]. To lead manufacturers to design and build more efficient IMs the European Union specified the new premium efficiency standard (IE3) for IMs operated at $50\,\mathrm{Hz}$ or $60\,\mathrm{Hz}$ by the IEC 60034-30 standard [3]. Since January 1, 2015 this standard is valid for IMs with a rated power of 7.5 to $375\,\mathrm{kW}$ and since January 1, 2017 for IMs with a rated power of 0.75 to $375\,\mathrm{kW}$. The standard also reserves an IE4 class for the future.

Due to the low-cost, ruggedness and fault tolerance, frequency-inverter-driven IMs are used as the main workhorse in the rising market of electrical and hybrid drive trains [4]. Here too, however, the main aim is to reduce the energy consumption or with other words to improve the efficiency of the drive train and particularly of the IM [5]. Moreover, in electric or hybrid vehicles minimum cost and weight are further goals [5]. Proficient manufacturers have the experience to design high premium efficient electrical machines. But only mathematical optimization can handle the complexity of the relations between the machine's geometry and it's performance and nonlinearity [6] in short time. With the mathematical optimization tool the limits can be pushed toward more efficient designs. For the design of high efficient IMs, particularly for frequency-inverter-driven ones, a detailed loss analysis is required. This requires local and temporal highly resolved nonlinear field computation and can be performed in the post processing of nonlinear transient finite element simulations of the magnetic circuit [7]. For the IM the finite-element-method (FEM) takes a large number of simulation time steps to build up the machine's rotor flux matrix [7]. Hence, using the time-consuming FEM in a mathematical optimization procedure would end up in an extremely time-consuming calculation and therefore is not suitable. Von Pfingsten, Nell and Hameyer [7], [8] proposed a hybrid simulation approach for IMs 2D-finite-element (FE) calculating that drastically decreases the simulation time by shortening the transient build-up of the rotor flux. Nevertheless, this hybrid appraoch, that needs about 2000 core hours for an efficiency map, is still not sufficient for the application in a mathematical optimization procedure. Due to the fact that the FEM and other numerical methods are very time-comsuming scaling laws are a popular method in physics and engineering. They are often used in numerous examples. Wood [9] described the general scaling laws for electromagnetic systems. His work was motivated by the constrain of the system's thermal stability. By using the electromagnetic and thermal diffusion equation and the momentum and kinematic equation Hsieh and Kim [10] presented a detailed derivation of scaling laws for electromechanical systems.

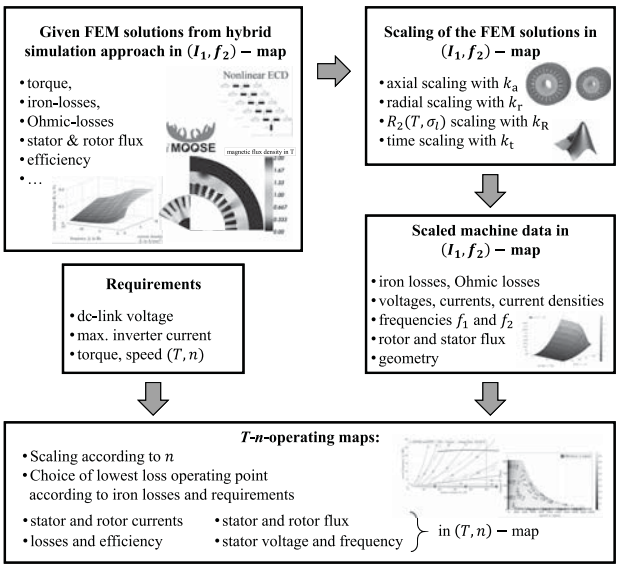

Fig. 1. Machine scaling scheme.

M. Nell, J. Lenz and K. Hameyer are with the Institute of Electrical Machines of RWTH Aachen University, Schinkelstr. 4, 52062 Aachen, Germany (e-mail: martin.nell@iem.rwth-aachen.de).

978-1-5386-2477-7/18/$31.00 ©2018 IEEE

Žarko, Stipetič and Ramakrishnan published several papers about the scaling laws for synchronous machines (SM). In [11] and [12] the procedures of radial and axial geometrical scaling and of rewinding for a SM are introduced. In [13] the efficiency maps of a SM are calculated by using a scalable saturated flux-linkage and loss model of a SM. In [5] and [14] the scalable SM models are used to find the optimal sizing of a SM traction motor. Moreover, Žarko presented a method to design premium efficiency IM using scaling laws for its equivalent circuit parameters in [2]. He assumed that the temperature rise in the slot of the original and the scaled motor are similar. An other method to improve the IM efficiency classes useing the method to scale the core axial lengthening was described by Alberti, Bianchi, Boglietti and Cavagnino in [15]. The influence or rotor diameter and length on the rating of IMs was presented by Bone in [16]. His scaling laws for IMs is not as exact as the ones derived in this paper because the field solutions change. Nonetheless, they are well applicable for machine designers.

In this paper a more sophisticated methodology for a mathematical optimization of squirrel cage IMs is discussed. It is based, one the one side, on the hybrid simulation approaches for induction machine calculation from von Pfingsten, Nell and Hameyer [7], [8] and on the other side on the scaling laws for IMs proposed in this paper. The procedure of this method is illustrated in Fig. 1. The I_1-f_2 - operation-maps of a reference machine design are calculated with the hybrid simulation approach of von Pfingsten, Nell and Hameyer [7], [8]. To obtain a new scaled motor design the solutions are scaled in the I_1-f_2 - map without changing the field solution of the IM. Taken into account requirements, such as dc-link voltage, maximum inverter current, and the operation strategy, such as Minimum-Torque-Per-Ampere (MTPA) or Minimum-Torque-Per-Electrical-Losses (MTPEL), the I_1-f_2 - maps are transformed into T-n - maps. Finally, the proposed method is used in an evolutionary optimization strategy to find the optimized IM size for a electric vehicle.

II. Modeling of an induction machine

A. IM operating points in terms of the I_1-f_2 - plane

The fundamental wave T-equivalent-circuit of an IM is presented in Fig. 2. It demonstrates the allocation of the stator current $\underline{I}_1$ into the magnetizing current $\underline{I}_\mu$ and the rotor current related to the stator side $\underline{I}_2^{\mathrm{s}}$. Moreover, it illustrates that all reactances and the rotor resistance R_2^{s} are proportional to the synchronous angular frequency ω_1. According to von Pfingsten, Nell and Hameyer in [8], [17] and [7] the allocation of the stator current $\underline{I}_1$ into the magnetizing current $\underline{I}_\mu$ and the rotor current $\underline{I}_2^{\mathrm{s}}$ is independent of the stator frequency f_1 by subtracting the voltage drop on the stator resistance R_1. As a result, this allocation only depends on the rotor frequency f_2 and the saturation of the main inductance L_{M}. The saturation has to be considered in highly utilized traction drives and occurs at high values of $\underline{I}_\mu$ that is reached at low values for f_2 and high values for $\underline{I}_1$ [17]. Therefore, the current allocation of $\underline{I}_1$ into $\underline{I}_\mu$ and $\underline{I}_2^{\mathrm{s}}$ only depends on the amplitude of the stator current $\underline{I}_1$ and the rotor current frequency f_2, as long as the rotor resistance and the inductances are assumed to be constant. All torque-speed-operating points of an IM with a constant rotor resistance R_2^{s} can be mapped in the stator current - slip frequency plane (I_1-f_2 - plane).

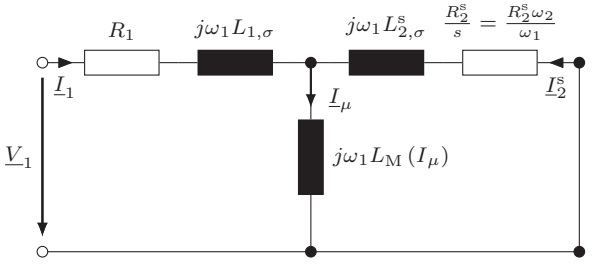

Fig. 2. Equivalent circuit diagram of a squirrel cage induction machine.

B. Induction machine calculation applying the hybrid simulation approach

To accelerate the FE-calculation of the IM the hybrid simulation approach presented in [7] and [8] is used. With the hybrid simulation approach the entire I_1-f_2 and T-n - map respectively can be calculated $50\,\%$ faster than the transient FEM. In combination with the hereafter introduced scaling scheme it provides a fast procedure to calculate and scale IMs, that leads to the possibility of the use for numerical optimization. The main aspects of it will be described in the following.

In a first step, a non-linear no-load static finite-element-analysis (FEA) with one simulation time step is conducted $k = 1...K$ times, where k marks a certain saturation state [8], [7]. The stator current $\underline{I}_1$ is the only excitation. For each non-linear no-load FEA the inductance matrix $\mathbf{L}(k)$ of the IM is extracted in accordance with [18]. From these extracted matrices $\mathbf{L}(k)$ the rotor current $\underline{I}_2^{\mathrm{s}}$ is calculated with the analytical fundamental-wave equations derived from the equivalent circuit diagram in Fig. 2 for every saturation state k. With the stator current vector $\vec{\underline{I}}_1$ and the saturation dependent rotor current vector $\vec{\underline{I}}_2^{\mathrm{s}}$ the stator flux linkage vector $\vec{\underline{\Psi}}_1(k)$ for every saturation state k is calculated. By comparing the amplitude of this stator flux linkage and the no-load stator flux linkage of the no-load FEA $\vec{\underline{\Psi}}_{1,\mathrm{nl}}(k)$ the valid saturation state is found. With a numerical interpolation the value of the rotor current for each operating point in the I_1-f_2-map is found and used as excitation for the second, now transient, FE-simulation [8], [7]. The calculation steps are performed in the I_1-f_2-plane with a fixed stator frequency f_1 and a fixed rotor resistance R_2^{s} and rotor conductivity σ_2 respectively. By considering an operation strategy, such as MTPEL, and by scaling the loss power of the IM according to different synchronous speeds f_1 as described in [4] the I_1-f_2-map is transformed into the T-n-map. A change of the rotor resistance R_2^{s} by temperature can be considered with the scaling laws of the rotor resistance due to temperature changes described in section III-C.

III. Scaling laws for an induction machine

The previous scaling laws for IMs introduced by Bone in [16] are not exact due to the fact that the field solution is changed. The IM scaling laws of Žarko in [2] deal with scaling the IM's equivalent circuit parameters assuming equal temperature rise in the slots of the original and reference motor. For the SM Stipetič, Žarko and Popescu derived scaling laws that consider the same field solution. This is the basis for the IM scaling laws in this paper. In the following the scaled parameters are marked with ($'$).

A. Geometrical scaling

The geometrical scaling in cylindrical systems is subdivided into radial and axial scaling with the radial scaling factor $\mathrm{k_r}$ and the axial scaling factor $\mathrm{k_a}$. The effect of the geometrical scaling is pictured in Fig. 3 described with

$$l^{'} = l\mathrm{k_a} \tag{1}$$

$$A^{'}_{\mathrm{cross}} = A_{\mathrm{cross}}\mathrm{k_r^2} \tag{2}$$

$$A^{'}_{\mathrm{surface}} = A_{\mathrm{surface}}\mathrm{k_r k_a} \tag{3}$$

$$V^{'} = V\mathrm{k_r^2 k_a} \tag{4}$$

where l is the axial length, A_{cross} the cross-section areas, A_{surface} the radial surface area and V the volume of the active part of the machine. The cross-section of the short-circuit ring also increases with $\mathrm{k_r^2}$ and is independent to $\mathrm{k_a}$ to preserve a constant relation to the bar cross-section. The conductor cross-section also changes with $\mathrm{k_r^2}$. For the endwindings it is assumed that the conductor length increases quadratically with $\mathrm{k_r}$ since conductor cross-sections increase and thus the axial extent becomes larger and the arc length increase linearly with $\mathrm{k_r}$.

B. Scaling of the electrical and magnetic parameters

Due to the fact that the magnetic permeability μ is in non-linear relation to the magnetic field strength $\vec{H}$ one assumption of scaling the FE-solutions is that the magnetic field strength distribution inside the IM does not change. Therefore, (5) is applicable. In accordance with Ampères Law (6) the scaling dependence of the electric current density $\vec{J}$ (7) follows, with the polar coordinates ρ and ϕ and the unit vector $\vec{\mathrm{e}}_{\mathrm{z}}$. Here, the assumption that the geometrical dimensions are clearly shorter than the magnetic wave length is used to get the simplified Ampères Law

$$\vec{H^{'}}(\rho^{'},\phi) = \vec{H}(\rho,\phi) \tag{5}$$

$$\vec{J^{'}} = \nabla^{'} \times \vec{H^{'}} \tag{6}$$

$$= \frac{1}{\rho^{'}}\left[\frac{\partial}{\partial\rho^{'}}(\rho^{'}H^{'}_{\phi}) - \frac{\partial H^{'}_{\rho}}{\partial\phi^{'}}\right]\vec{\mathrm{e}}_{\mathrm{z}}$$

$$\vec{J^{'}} = \frac{1}{\mathrm{k_r}}\left(\nabla \times \vec{H}\right) = \frac{1}{\mathrm{k_r}}\vec{J} \tag{7}$$

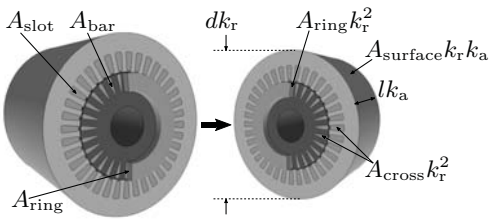

Fig. 3. Scaled machine parameter.

In [10] it is described that a scaling factor $\mathrm{k_{t1}}$ has to be used to satisfy that the magnetic flux density B is kept constant $B(\rho,\phi) = B^{'}\left(\rho^{'},\phi^{'}\right)$ and therefore the equality of the magnetic field strength (5) is satisfied. With Faraday's law of induction (8), (9) can be transformed in (10), where σ is the electric conductivity and $\vec{\mathrm{E}}$ the electric field strength. The assumption that the magnetic field strength and therefore the magnetic flux density do not change during scaling lead to (11). Hence, the time scaling factor $\mathrm{k_{t1}}$ corresponds to the square of the radial scaling factor $\mathrm{k_r}$. As a result, all time depending parameters have to be scaled by the total time scaling factor $\mathrm{k_t}$, which is the product of the first time scaling factor $\mathrm{k_{t1}}$ and the second one $\mathrm{k_{t2}}$. The second time scaling factor is a result of the rotor resistance scaling and will be discussed in detail in section III-C. The time scaling leads to the proportionality of the reactances to the reciprocal time scaling factor shown in Fig. 4.

$$\nabla \times \vec{\mathrm{E}} = \frac{\partial\vec{B}}{\partial t} \tag{8}$$

$$\nabla \times \vec{H} = \sigma\vec{\mathrm{E}} \tag{9}$$

$$\mathrm{k_{t1}}\frac{\partial\vec{B}^{'}}{\partial t^{'}} + \mathrm{k_r^2}\nabla^{'} \times \frac{1}{\sigma}(\nabla^{'} \times \frac{\vec{B}^{'}}{\mu}) = 0 \tag{10}$$

$$\mathrm{k_{t1}} = \mathrm{k_r^2} \tag{11}$$

The magnetic flux Ψ, which is proportional to the inductance $(\mathrm{k_a})$ and the current $(\mathrm{k_r})$, changes with $\mathrm{k_a k_r}$ (see (12)). From (2) and (7) it follows that the current changes with $\mathrm{k_r}$ (see (13)). The machine's torque T_{elec} is dependent to the flux and current. Hence, the torque is scaled in accordance to (14).

$$\Psi^{'} = \mathrm{k_r k_a}\Psi \tag{12}$$

$$I^{'} = \mathrm{k_r}I \tag{13}$$

$$T^{'}_{\mathrm{elec}} = \frac{3}{2}p(I_{\mathrm{q},1}\mathrm{k_r}\Psi_{\mathrm{d},1}\mathrm{k_r k_a} - I_{\mathrm{d},1}\mathrm{k_r}\Psi_{\mathrm{q},1}\mathrm{k_r k_a})$$

$$= T_{\mathrm{elec}}\mathrm{k_r^2 k_a} \tag{14}$$

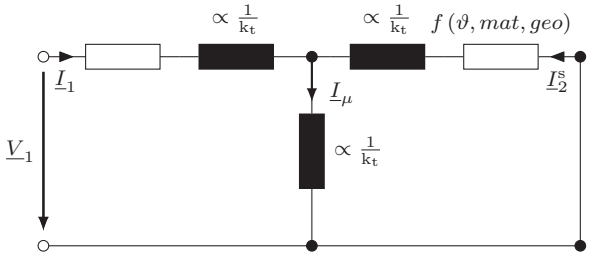

Fig. 4. Scaling factor dependencies of the elements of the equivalent circuit diagram of a squirrel cage induction machine.

C. Rotor resistance scaling due to geometric changes

The equivalent circuit of the IM in Fig. 2 shows that the rotor resistance related to the stator side R_2^{s} and therefore the rotor resistance R_2 has a major impact on the machine's behavior. In contrast to the scaling of the SM done by Žarko, Stipetič and Ramakrishnan in IMs the scaling of the rotor resistance is an important step. In addition to the changed rotor resistance due to the geometrical scaling the resistance can vary due to temperature and material and electric conductivity variations respectively. The consequence of the geometrical scaling has to be considered separately in terms of the bar resistance R_{bar} and the resistance of the short-circuit ring R_{ring}^{*}. The resistance of a rotor bar can be described with

$$R_{\mathrm{bar}} = \frac{l_{\mathrm{Fe}}}{\sigma_2 A_{\mathrm{bar}}} \propto \frac{\mathrm{k_a}}{\mathrm{k_r^2}}, \tag{15}$$

where l_{Fe} is the active length of the IM, A_{bar} the area of a rotor bar and σ_2 the conductivity of the rotor cunductors, and is proportional to $\mathrm{k_a/k_r^2}$. The resistance of a short-circuit-ring-segment ΔR_{ring} can be described by

$$\Delta R_{\mathrm{ring}} = \frac{2\pi r_{\mathrm{ring}}}{\sigma_2 A_{\mathrm{ring}} Q_2} \propto \frac{\mathrm{k_r}}{\mathrm{k_r^2}} = \frac{1}{\mathrm{k_r}}, \tag{16}$$

where r_{ring} describes the middle radius of the short-circuit ring, A_{ring} the area of the short-circuit ring and Q_2 the rotor bar number. According to [19] this resistance can be transformed into an equivalent series resistance $\Delta R_{\mathrm{ring}}^{*}$ described by

$$\Delta R_{\mathrm{ring}}^{*} = \Delta R_{\mathrm{ring}} \cdot \frac{1}{\left(2\sin\left(\frac{\pi p}{Q_2}\right)\right)^2} \propto \frac{1}{\mathrm{k_r}}, \tag{17}$$

with the number of pole-pairs p, which is used in the 2D-FEM. As outlined in section III-A the cross-section area of the short-circuit ring increases with $\mathrm{k_r^2}$ and is independent to the axial scaling. Therefore, $\Delta R_{\mathrm{ring}}^{*}$ is proportional to the inverse of the radial scaling factor $\mathrm{k_r}$ as in (17). The addition of the bar resistance and the equivalent series resistance of the short-circuit ring lead to the total resistance of the rotor

$$R_2 = R_{\mathrm{bar}} + 2\Delta R_{\mathrm{ring}}^{*}. \tag{18}$$

By defining a compensating conductivity

$$\sigma_{2,\mathrm{comp}} = \frac{l_{\mathrm{Fe}}}{A_{\mathrm{bar}} R_2} \propto \frac{\mathrm{k_a}}{\mathrm{k_r^2} \cdot \mathrm{k}\left(R_2\right)} \tag{19}$$

it leads to a rotor resistance scaling factor

$$\mathrm{k_{R1}} = \frac{\sigma_{2,\mathrm{comp}}}{\sigma_{2,\mathrm{comp}}^{'}} = 1 + \left(\frac{\mathrm{k_r}}{\mathrm{k_a}} - 1\right)\kappa_2 \tag{20}$$

$$\text{with} \quad \kappa_2 = \frac{1}{\frac{l_{\mathrm{Fe}}}{\pi r_{\mathrm{ring}}}\frac{A_{\mathrm{ring}}}{A_{\mathrm{bar}}} Q_2 \sin^2(\pi p/Q_2) + 1}$$

as the rotor geometry constant that is defined for the unscaled machine.

D. Rotor resistance scaling due to rotor conductivity variations

The scaling of the rotor resistance in accordance to the scaling of the compensating rotor conductivity leads to further possibilities of rotor resistance scaling. The rotor conductivity and resistance respectively can vary due to a change of the material or by temperature. Hence, a second rotor resistance scaling factor $\mathrm{k_{R2}}$ is introduced in (21). It is dependent on the old and new conductivity, σ_2 and $\sigma_{2,\mathrm{new}}$, the old and new temperature coefficients α and α_{new}, the old and new reference temperatures ϑ_{ref} and $\vartheta_{\mathrm{ref,new}}$ and the old and new simulation temperatures ϑ_{sim} and $\vartheta_{\mathrm{sim,new}}$.

$$\mathrm{k_{R2}} = \frac{\sigma_2}{\sigma_{2,\mathrm{new}}} \frac{1 + \alpha_{\mathrm{new}}\left(\vartheta_{\mathrm{sim,new}} - \vartheta_{\mathrm{ref,new}}\right)}{1 + \alpha\vartheta\left(\vartheta_{\mathrm{sim}} - \vartheta_{\mathrm{ref}}\right)} \tag{21}$$

The resulting scaling factor for the rotor resistance can be calculated by the the total scaling factor of the rotor resistance $\mathrm{k_R}$ and leads to the scaled rotor resistance:

$$R_2^{'} = R_2 \mathrm{k_R} \quad \text{with} \quad \mathrm{k_R} = \mathrm{k_{R1}} \mathrm{k_{R2}} \frac{\mathrm{k_a}}{\mathrm{k_r^2}}. \tag{22}$$

Fig. 4 shows that the rotor resistance is dependent on the temperature, material and geometry of the IM. To satisfy (5) the allocation of $\underline{I}_2^{\mathrm{s}}$ and $\underline{I}_{\mu}$ must not vary. As long as the rotor resistance is kept constant and the calculation of the machine is done in the I_1-f_2 - plane as described in section II-A (5) is valid. With a change in R_2 the allocation changes. To keep the same current allocation a second time scaling factor

$$\mathrm{k_{t2}} = \frac{\mathrm{k_a}}{\mathrm{k_R k_{t1}}} = \frac{1}{\mathrm{k_{R1} k_{R2}}} \tag{23}$$

is established. Thus, the total time scaling factor results in

$$\mathrm{k_t} = \mathrm{k_{t1} k_{t2}}. \tag{24}$$

With these rotor scaling factors it is possible to scale the IM due to a change of the rotor resistance. This change can be a result of a variation in the conductivity of the rotor conductor by different materials, such as copper or aluminum, or by their different qualities, as well as by an alternating temperature. Differences in the machine's behavior due to a changing quality of the rotor bar material can be calculated very fast with the proposed scaling process. In addition a change of the rotor resistance due to the skin effect can be taken into account by using analytical formula to recalculate the rotor resistance. This scaling process can also be used in combination with a thermal model of the IM to simulate the machine in different operating points with changing temperature conditions.

E. Scaling of the IM losses

The losses of an IM can be distinguished in Ohmic losses $P_{\mathrm{L,ohm}}$ and iron losses $P_{\mathrm{L,Fe}}$. The Ohmic losses are proportional to $\mathrm{k_r^2 k_R}$ as in (25).

$$P_{\mathrm{L,ohm,2}}^{'} = P_{\mathrm{L,ohm,2}} \mathrm{k_r^2 k_R} \tag{25}$$

The iron losses, in turn, can be separated into hysteresis, eddy current and excess losses [17]. All three parts have a different dependency on the frequency f.

Hence, different scaling relations for the three iron loss components exist. The iron loss power density $p_{\mathrm{L,Fe}}$ is

$$p_{\mathrm{L,Fe}}^{'} = \left(k_{\mathrm{hyst}} B^{\alpha} \frac{f}{\mathrm{k_t}} + k_{\mathrm{eddy}} B^2 \frac{f^2}{\mathrm{k_t^2}} + k_{\mathrm{excess}} B^{1.5} \frac{f^{1.5}}{\mathrm{k_t^{1.5}}} \right) \tag{26}$$

where k_{hyst}, k_{eddy} and k_{excess} are the hysteresis loss, eddy current loss and excess loss coefficient respectively. With the iron loss power density and the iron mass m_{Fe}, scaled with $\mathrm{k_r^2 k_a}$, the scaled iron loss power $P_{\mathrm{L,Fe}}^{'}$ is

$$P_{\mathrm{L,Fe}}^{'} = p_{\mathrm{L,Fe}}^{'} m_{\mathrm{Fe}} \mathrm{k_r^2 k_a}. \tag{27}$$

All scaling laws for the IM are summarized in table I.

parameter	**variable**	$\propto$
length	l	$\mathrm{k_a}$
lateral surface	A_{surface}	$\mathrm{k_a\ k_r}$
cross sectional area	A_{cross}	$\mathrm{k_r^2}$
volume	V	$\mathrm{k_a k_r^2}$
magnetic field strength	H	1
magnetic flux density	B	1
magnetic flux linkage	Ψ	$\mathrm{k_a k_r}$
current density	J	$\frac{1}{\mathrm{k_r}}$
current	I	$\mathrm{k_r}$
time	t	$\mathrm{k_t}$
frequency	f	$\frac{1}{\mathrm{k_t}}$
speed	n	$\frac{1}{\mathrm{k_t}}$
torque	T	$\mathrm{k_a k_r^2}$
voltage	V	$\frac{\mathrm{k_a k_r}}{\mathrm{k_t}}$
inductance	L	$\mathrm{k_a}$
reactance	X	$\frac{\mathrm{k_a}}{\mathrm{k_t}}$
rotor resistance	R_2	$\mathrm{k_R}$
mechanical power	P_{mech}	$\frac{\mathrm{k_a k_r^2}}{\mathrm{k_t}}$
mechanical power density	p_{mech}	$\frac{1}{\mathrm{k_t}} = \frac{\mathrm{k_R}}{\mathrm{k_a}}$

TABLE I
SCALING FACTORS FOR THE MACHINE'S PARAMETER.

F. Validation of the scaling laws

To validate the scaling laws for IMs a reference motor is calculated with FEM in a first step via the hybrid simulation approach described in section II-B. In a second step, the geometry and the rotor resistance of the IM are scaled and a second FE-simulation is performed with the scaled machine. The scaling factors in this steps are, $\mathrm{k_r} = 1.2$, $\mathrm{k_a} = 1.1$ and $\mathrm{k_R} = 1.05$. In a third step, the FE-solutions of the scaled IM are rescaled in the I_1-f_2-plane to the parameters of the reference machine regarding the procedure described in Fig. 1. The results of FE-solutions of the reference machine (first step) and the rescaled FE-solutions of the scaled machine (third step) are compared. The comparison is done in the I_1-f_2-plane. Fig. 5 shows the calculated deviation of the loss power in %. The maximum error is $-17 \cdot 10^{-3}\%$, that proves the correctness of the proposed scaling scheme.

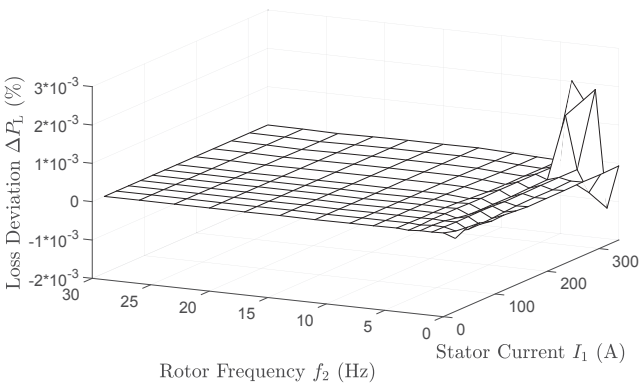

Fig. 5. Total loss deviation of the reference and the rescaled FE-solutions in the I_1-f_2-plane.

In Fig. 6 the total losses transformed to the T-n-map of the scaled and the rescaled IM machine FE-solutions are shown. For the transformation of the FE-solutions into the T-n-map the same requirements, such as the maximum frequency inverter current and the maximum dc-link voltage and the operation strategy MTPEL, are taken into account. The comparison of the reference loss power and the loss power of the IM rescaled in the I_1-f_2-map and transformed into the T-n-map is presented in Fig. 7. It also shows a very accurate performance of the proposed scaling procedure.

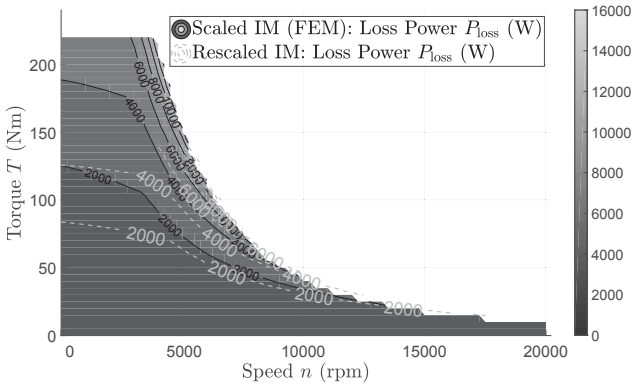

Fig. 6. Total losses of the FE-solutions of the reference and scaled machine.

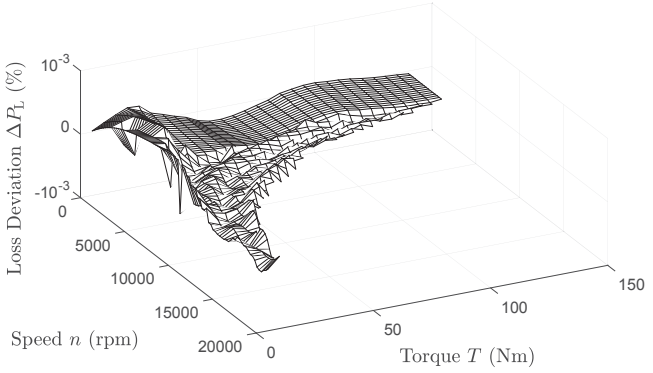

Fig. 7. Total loss deviation of the reference and the rescaled FE-solutions in the T-n-map.

IV. Optimization of an induction machine for traction application

Due to its very fast performance the proposed machine scaling scheme can be used in numerical optimization procedure. In [20] Stipetič and Žarko present an overview of the methodology using mathematical optimization procedures to achieve an optimal design of an electrical machine. They suggest meta-heuristic algorithm, such as Evolution Strategy or Differential Evolution, for the complex electrical machine design. In [14] a mixed integer distributed ant colony optimization is used to optimize a traction drive with a permanent magnet motor calculated by using FEM and geometrical scaling. In [21] a multi objective optimization in combination with the scaling laws of a SM is used to find the optimal size of the traction motor as it is done in [5] with the gear ratio as an additional design variable.

A. Methodology

To show the potential and usability of the proposed IM scaling scheme an IM in an electric vehicle is optimized. Changes of the machine configuration, like number of stator slots, are not considered to focus on the radial and axial scaling. As the design parameters the gear ratio, the axial length and the radius of the IM are used. The objective function that is minimized in the optimization process considers the costs of the machine and the produced loss energy of the IM in the Worldwide harmonized Light vehicles Test Procedure (WLTP). Here, the costs of the machine and the loss energy are weighted with different factors.

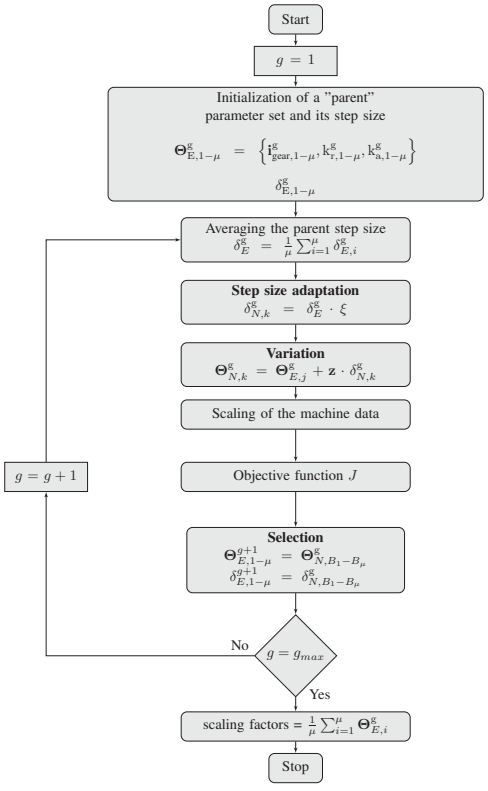

Fig. 8. Evolutionary Strategy.

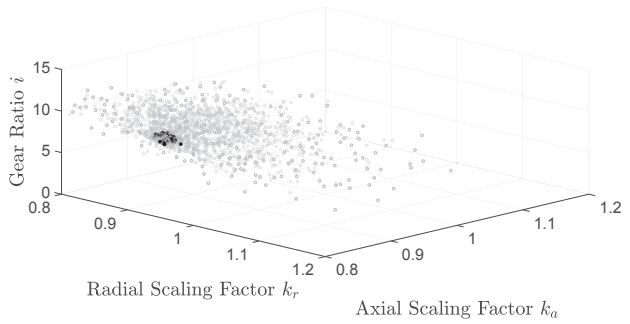

Fig. 9. Pareto front of the proposed optimization process.

It starts with the initialization of the parameter set $\boldsymbol{\Theta}^{\mathrm{g}}_{\mathrm{E},1-\mu}$ and the step size of the parameters $\delta^{\mathrm{g}}_{\mathrm{E},1-\mu}$, where μ is the number of the parents and g the generation number. For the initial parameters the radial and axial scaling factor are set to $\mathrm{k_r} = \mathrm{k_a} = 1$ and the gear ratio is set to $i_{\mathrm{gear}} = 8$. The initial step size is set to a fourth of the initial parameter values. The step size is averaged in the second step and adapted by a logarithmic distributed random number. With the normal distributed random number z and the step size the new parameter sets $\boldsymbol{\Theta}^{\mathrm{g}}_{N,k}$, named progenies, are calculated in the variation step.

With the new parameters the machine is scaled, the gear ratio changed and the objective function is calculated. In the selection the best progenies become the new parents parameter and the calculation of the next generation is started. The process ends after a certain number of generations.

B. Results

The results of the design optimization with the Evolutionary strategy is shown in Fig. 9. It shows the pareto front in dependence of the radial scaling factor $\mathrm{k_r}$, the axial scaling factor $\mathrm{k_a}$ and the gear ratio i_{gear}. All different parameter sets are marked with a gray point. The pareto optimum is marked by black dots. It can be seen that the optimization algorithm varies the three variable parameters in a wide range and converge fast towards an optimum region. The calculation of the objective function for every single parameter set, including the scaling of the IM's FE-solutions, in Matlab takes a processor time of ca. $0.8\,\mathrm{s}$, using an Intel(R) Core(TM) i7-6500U CPU @ $2.5\,\mathrm{GHz}$ and a 8 GB RAM.

V. Conclusions and further work

In this paper an IM scaling procedure for the machine's 2D-FE-solutions is proposed. Besides the geometrical scaling of the IM, the scaling laws for changes in the rotor resistance is presented. The reference FE-solutions of an IM, calculated by a hybrid IM simulation approach, are scaled in the I_1-f_2-map and transformed into the T-n-map, by considering boundary condition, such as maximum current, and taking into account an operation strategy. The results of the scaling process show a very good agreement with the FE-results of a scaled IM. The scaling procedure is tested in an optimization

of a traction drive. The results of the optimization show that the proposed scaling process is suitable for the use in numerical optimization processes. It can be well applied in the design optimization of traction drive or other application-related optimizations including driving cycles. The rotor resistance scaling can be used to analyze the machine's behavior for different rotor bar materials or their quality differences. It can also be used in combination with a thermal model of the IM to calculate the IM in difference temperature conditions. The proposed scaling methodology is a rapid and very accurate tool to scale entire operation maps of IMs. In further work, the scaling laws for rewinding and for changes in the electrical steel due to temperature differences or the quality of the material will be studied. Furthermore, the limits of this method will be analyzed and the scaling will be validated for different machine configurations and designs, such as closed rotor slots. A validation with experimental results will be conducted. The focus of further publications can also be the optimization process itself, the searching algorithm and including different machine configurations in the optimization procedure.

REFERENCES

[1] S. Mallik, K. Mallik, A. Barman, D. Maiti, S. K. Biswas, N. K. Deb, and S. Basu, "Efficiency and cost optimized design of an induction motor using genetic algorithm," *IEEE Transactions on Industrial Electronics*, vol. 64, no. 12, pp. 9854–9863, Dec 2017.

[2] D. ZARKO, "Design of premium efficiency (ie3) induction motors using evolutionary optimization and scaling laws," vol. 1, pp. 183–186, 12 2016.

[3] S. Einfuegen, "Efficiency and cost optimized design of an induction motor using genetic algorithm," *IEEE Transactions on Industrial Electronics*, vol. 64, no. 12, pp. 9854–9863, Dec 2017.

[4] G. V. Pfingsten, S. Steentjes, and K. Hameyer, "Operating point resolved loss calculation approach in saturated induction machines," *IEEE Transactions on Industrial Electronics*, vol. 64, no. 3, pp. 2538–2546, March 2017.

[5] K. Ramakrishnan, S. Stipetič, M. Gobbi, and G. Mastinu, "Multi-objective optimization of electric vehicle powertrain using scalable saturated motor model," in *2016 Eleventh International Conference on Ecological Vehicles and Renewable Energies (EVER)*, April 2016, pp. 1–6.

[6] D. Žarko, S. Stipetič, M. Martinovic, M. Kovačić, T. Jercic, and Z. Hanic, "Reduction of computational efforts in finite element-based permanent magnet traction motor optimization," *IEEE Transactions on Industrial Electronics*, vol. 65, no. 2, pp. 1799–1807, Feb 2018.

[7] G. von Pfingsten, M. Nell, and K. Hameyer, "Hybrid simulation methods for induction machine calculation reduction of simulation effort by coupling static fea with transient fea and analytic formulations," in *2017 18th International Symposium on Electromagnetic Fields in Mechatronics, Electrical and Electronic Engineering (ISEF) Book of Abstracts*, Sept 2017, pp. 1–2.

[8] G. von Pfingsten and K. Hameyer, "Highly efficient approach to the simulation of variable-speed induction motor drives," *IET Science, Measurement Technology*, vol. 11, no. 6, pp. 793–801, 2017.

[9] R. W. Wood, "Scaling magnetic systems," *IEEE Transactions on Magnetics*, vol. 47, no. 10, pp. 2685–2688, Oct 2011.

[10] K. T. Hsieh and B. K. Kim, "One kind of scaling relations on electromechanical systems," *IEEE Transactions on Magnetics*, vol. 33, no. 1, pp. 240–244, Jan 1997.

[11] S. Stipetič, D. Žarko, and M. Popescu, "Scaling laws for synchronous permanent magnet machines," in *2015 Tenth International Conference on Ecological Vehicles and Renewable Energies (EVER)*, March 2015, pp. 1–7.

[12] ——, "Ultra-fast axial and radial scaling of synchronous permanent magnet machines," *IET Electric Power Applications*, vol. 10, no. 7, pp. 658–666, 2016.

[13] S. Stipetič and J. Goss, "Calculation of efficiency maps using scalable saturated flux-linkage and loss model of a synchronous motor," in *2016 XXII International Conference on Electrical Machines (ICEM)*, Sept 2016, pp. 1380–1386.

[14] D. Žarko, M. Kovačić, S. Stipetič, and D. Vuljaj, "Optimization of electric drives for traction applications," in *2017 19th International Conference on Electrical Drives and Power Electronics (EDPE)*, Oct 2017, pp. 15–32.

[15] L. Alberti, N. Bianchi, A. Boglietti, and A. Cavagnino, "Core axial lengthening as effective solution to improve the induction motor efficiency classes," *IEEE Transactions on Industry Applications*, vol. 50, no. 1, pp. 218–225, Jan 2014.

[16] J. C. H. Bone, "Influence of rotor diameter and length on the rating of induction motors," *Electric Power Applications, IEE Journal on*, vol. 1, no. 1, pp. 2–6, February 1978.

[17] G. von Pfingsten, S. Steentjes, and K. Hameyer, "Transient approach to model operating point dependent losses in saturated induction machines," in *2016 XXII International Conference on Electrical Machines (ICEM)*, Sept 2016, pp. 626–632.

[18] E. Lange, F. Henrotte, and K. Hameyer, "An efficient field-circuit coupling based on a temporary linearization of fe electrical machine models," *IEEE Transactions on Magnetics*, vol. 45, no. 3, pp. 1258–1261, March 2009.

[19] S. Williamson and M. C. Begg, "Calculation of the resistance of induction motor end rings," *IEE Proceedings B - Electric Power Applications*, vol. 133, no. 2, pp. 54–60, March 1986.

[20] S. Stipetič, W. Miebach, and D. Žarko, "Optimization in design of electric machines: Methodology and workflow," in *2015 Intl Aegean Conference on Electrical Machines Power Electronics (ACEMP), 2015 Intl Conference on Optimization of Electrical Electronic Equipment (OPTIM) 2015 Intl Symposium on Advanced Electromechanical Motion Systems (ELECTROMOTION)*, Sept 2015, pp. 441–448.

[21] K. Ramakrishnan, S. Stipetič, M. Gobbi, and G. Mastinu, "Optimal sizing of traction motors using scalable electric machine model," *IEEE Transactions on Transportation Electrification*, vol. PP, no. 99, pp. 1–1, 2017.

VI. BIOGRAPHIES

Martin Nell was born in Koblenz in Germany, on July 11, 1990. He recieved his Bachelor's degree in October 2014 and his Master's degree in April 2017 in electrical engineering from RWTH Aachen University, Germany.
He has been working as a research associate at the Institute of Electrical Machines since May 2017. His research interests include induction machine modelling, optimization of induction machines, iron loss calculation in macroscopic scale and vehicle modelling.

Jonas Lenz was born in Gießen in Germany, on December 10, 1991. He recieved his Bachelor's degree in September 2016 in electrical engineering from RWTH Aachen University, Germany.
He has been working on his master thesis "Development of a scalable numerical machine model of an induction machine" at the Insitute of Electrical Machines since October 2017.

Dr. Kay Hameyer received his M.Sc. degree in electrical engineering from the University of Hannover and his Ph.D. degree from the Berlin University of Technology, Germany. After his university studies he worked with the Robert Bosch GmbH in Stuttgart, Germany as a Design Engineer for permanent magnet servo motors and vehicle board net components. Until 2004 Dr. Hameyer was a full Professor for Numerical Field Computations and Electrical Machines with the KU Leuven in Belgium. Since 2004, he is full professor and the director of the Institute of Electrical Machines (IEM) at RWTH Aachen University in Germany. 2006 he was vice dean of the faculty and from 2007 to 2009 he was the dean of the faculty of Electrical Engineering and Information Technology of RWTH Aachen University. His research interests are numerical field computation and optimization, the design and controls of electrical machines, in particular permanent magnet excited machines, induction machines and the design employing the methodology of virtual reality. Since several years Dr. Hameyers work is concerned with the magnetic levitation for drive systems, magnetically excited audible noise in electrical machines and the characterization of ferro-magnetic materials. Dr. Hameyer is author of more than 250 journal publications, more than 500 international conference publications and author of 4 books. Dr. Hameyer is a member of VDE, IEEE senior member, fellow of the IET.